



Aluminium chloride: A new aluminium source to prepare SAPO-34 catalysts with enhanced stability in the MTO process

Teresa Álvaro-Muñoz*, Carlos Márquez-Álvarez, Enrique Sastre

Instituto de Catálisis y Petroleoquímica, ICP-CSIC, C/Marie Curie, 2, 28049 Madrid, Spain



ARTICLE INFO

Article history:

Received 26 July 2013

Received in revised form

28 November 2013

Accepted 11 December 2013

Available online 17 December 2013

Keywords:

MTO

SAPO-34 nanocrystals

Aluminium chloride

Dilute precursor solutions

ABSTRACT

The MTO process produces lower olefins from natural gas or coal via methanol, providing an interesting route to obtain valuable petrochemicals from carbon sources alternative to petroleum. Small-pore silicoaluminophosphate SAPO-34 has been proven an efficient catalyst for the MTO process, showing exceptionally high selectivity to lower olefins. However, these catalysts undergo rapid deactivation due to deposition of high molecular weight hydrocarbons on the pore entrances, which completely blocks the internal channels of the SAPO-34 crystals. In the present work, we explore the use of very dilute zeotype precursor solutions to reduce the size of the crystals of these materials, improving greatly their catalytic behaviour in the MTO process by increasing the catalyst life time.

© 2013 Elsevier B.V. All rights reserved.

1. Introduction

The global energy crisis has renewed the interest in developing technologies to produce energy, fuels and chemicals from resources other than traditional fossil fuels (oil, coal, gas). A large number of base chemicals are carbon-containing compounds (in many cases obtained from olefins), so alternative sources for their production are very limited. It is not necessary to emphasize the importance of petroleum in global economy at present. It is mainly used as source of fuels in energy production plants, as an energy source in domestic and industrial uses, in transportation, but also, although in a much lesser extent, as raw material in chemicals synthesis. The petroleum transformation represents a large percentage of the total chemical processes, despite the huge problem associated to the limited known global reserves, which are not expected to increase in the short-term. Therefore, due to the high oil prices and limitation of resources, it is necessary to develop new processes for the production of compounds that are traditionally derived from certain petroleum fractions.

Light olefins such as ethylene, propylene and butylenes are important intermediates for the petrochemical industry. They can be produced via several processes using mainly fossil, and therefore non-renewable, raw materials. In this sense, the production of light olefins from methanol (Methanol-to-Olefins or MTO process)

is an attractive synthesis route because methanol can be obtained from a wide variety of materials.

Methanol can be efficiently produced from syngas [1–3] obtained by natural gas reforming or carbon gasification, and it might even provide an environmentally carbon neutral alternative to fossil carbon sources [4], if produced by chemical recycling of carbon dioxide via hydrogenation [5] or from syngas obtained by biomass gasification [6].

Small-pore silicoaluminophosphate SAPO-34 (chabazite framework type) has been proven an efficient catalyst for the MTO process. This catalyst is exceptionally selective to lower olefins (selectivities over 80% to C_2^- – C_4^- olefins have been obtained) [7,8] because it has small pore entrances which allow only the diffusion of linear hydrocarbons thus inhibiting production of aromatic hydrocarbons. However, the main drawback of this catalyst is its rapid deactivation. Deactivation starts when aromatics and heavy branched compounds are formed inside the large cages. These molecules cannot diffuse through the porous structure of the catalyst because their kinetic diameter is larger than the pore-opening size. Therefore, they remain inside the cages where they can form carbonaceous deposits that block the pore openings and prevent the access of molecules to the active sites [9,10]. Coke compounds may adsorb on the acid sites, poisoning the catalyst active centres. Olsbye and col. studied the deactivation process of several zeolitic materials in the methanol-to-hydrocarbons (MTH) and MTO processes [11–14]. They concluded that the formation of coke during the MTO reaction on ZSM-5 crystals significantly differs from that on SAPO-34 crystals. Pore blocking in ZSM-5 zeolite has

* Corresponding author. Tel.: +34 915854796.

E-mail address: teresa.alvaro@icp.csic.es (T. Álvaro-Muñoz).

Table 1

Synthesis conditions used to prepare SAPO materials from gels with molar composition $1\text{Al}_2\text{O}_3:1\text{P}_2\text{O}_5:0.6\text{SiO}_2:x\text{TEAOH}:y\text{H}_2\text{O}$. Crystallization was maintained at 423 K for 5 days.

Catalyst	<i>x</i>	<i>y</i>	Silicon source ^b	pH gel	pH cryst	Phase
$\text{Al}(\text{OH})_3\text{-L}^{\text{a}}$	1	40	L	6.8	7.3	Chabazite
$\text{AlCl}_3\text{-L-3}$	3	65	L	1.4	0.2	Cristobalite
$\text{AlCl}_3\text{-L-6}$	6	110	L	8.5	9.3	Chabazite
$\text{AlCl}_3\text{-T-6}$	6	110	T	8.5	8.4	Chabazite

^a Reference sample synthesized with aluminium hydroxide [21].

^b L: Ludox; T: TEOS.

been related to the formation of polycyclic aromatic compounds at the channel intersections or on the outer surface, while in SAPO-34 it arises from polycyclic aromatic molecules formed in the large cavities. Both processes lead to catalyst deactivation [15,16] but the differences in pore architecture of these materials affect the coke formation and therefore the activity of the catalyst. In this respect, ZSM-5, although less sensitive to deactivation as compared to SAPO-34, has a low selectivity towards light olefins.

Numerous studies indicate that the morphology of SAPO-34 crystals can affect their properties and applications and various methods have been suggested to improve catalyst lifetime in the MTO reaction [9,17–21]. Catalyst deactivation may be strongly correlated with particle size due to the diffusion limitations of the guest molecules in the micropores [22]. For large catalyst crystals, residence time for hydrocarbons is high because of the long diffusion path. Aromatic compounds cannot escape from the pores of SAPO-34 and successive polymerizations readily occur because of the long reaction time. Chen et al. [9] examined the effect of crystal size of SAPO-34 on its selectivity and deactivation in the MTO reaction. In large crystals, the reactions were controlled by limitations in the diffusion of both methanol and the intermediate product dimethyl ether (DME). Furthermore, the coking rate increased with increasing crystal size. It was found that SAPO-34 catalysts with crystal size of less than 500 nm showed remarkable lifetime in the MTO reaction. Lee et al. used various templates to obtain SAPO-34 catalysts with similar physico-chemical properties but different crystal size and discussed the effect of crystal size on the catalytic performance, especially on deactivation behaviour [20]. They concluded that deactivation is related to diffusion limitation and that catalysts with smaller crystal size show slower deactivation due to the higher proportion of accessible cages near the external surface. Yao et al. [23] reported a polymer-assisted dry gel synthesis method aiming to control crystal growth. Using this approach, SAPO-34 nanocrystals were successfully formed from a precursor gel containing polyacrylamide, but SAPO-34 crystals larger than several micrometres were also formed simultaneously.

Other authors have tried to improve the diffusivity of the products creating hierarchical pores into the SAPO-34 crystallites by different synthesis methods [24,25] or using carbon materials (nanoparticles, nanotubes) as templates [26]. In all these cases an important improvement in the lifetime of the catalysts was observed.

The above mentioned reports suggest that control of the size of SAPO-34 crystals is a very important factor for improving the catalytic activity and lifetime of the catalyst. However, small SAPO-34 crystals with a uniform particle size have been obtained mainly through fractionation of the products. In this sense, nowadays several attempts to synthesize SAPO-34 and other zeolitic and mesoporous materials with small crystal size have been carried out using different approaches: synthesis from colloidal solutions [27,28] or applying microwave heating [28–33].

One promising route for preparation of microporous and particularly zeolite nanocrystals is the use of clear solutions or colloidal suspensions as precursor media. A review summarizing the different systems studied was published from Tosheva and Valtchev

[34]. This article mainly deals with zeolite synthesis, but also aluminophosphate systems, namely, AlPO-5 (AFI), AlPO-11 (AEL), and AlPO-18 (AEI), are discussed. In the present work, we explore the use of very dilute zeotype precursor solutions to obtain SAPO-34 with decreased crystal size, which is shown to improve its catalytic performance.

2. Experimental

2.1. Synthesis of SAPO-34 molecular sieves

Hydrothermal synthesis of SAPO-34 samples was carried out using tetraethylammonium hydroxide as template and aluminium chloride as aluminium source. The gel composition was: $1\text{Al}_2\text{O}_3:1\text{P}_2\text{O}_5:0.6\text{SiO}_2:x\text{TEAOH}:y\text{H}_2\text{O}$. The molar composition of the reaction mixtures and the synthesis conditions for the different SAPO-34 materials obtained are given in Table 1. For comparative purposes, a reference material was synthesized by the conventional procedure, using $\text{Al}(\text{OH})_3$ as aluminium source, according to the method published previously [21]. Experimental conditions (temperature and crystallization times) have been adjusted in order to obtain pure phases of SAPO-34. The same silicon to aluminium ratio (0.3) was used for all the synthesis gels prepared.

In a typical synthesis to get pure SAPO-34, the aluminium source (aluminium chloride, 99% or aluminium hydroxide, reagent grade, both from Sigma Aldrich) was added slowly to a dilute phosphoric acid solution (prepared using orthophosphoric acid, Riedel de Haen, 85%), and the mixture was vigorously stirred for 2 h to obtain a uniform gel. Silica solution (Sigma-Aldrich, Ludox SM-30, 30 wt% suspension in water) or tetraethylorthosilicate (TEOS, Merck, 98%) was added dropwise to this mixture, followed by addition of the template, tetraethylammonium hydroxide (TEAOH, Sigma-Aldrich, 35 wt% in water). Finally, the mixture was stirred for about 4 h. The gel was then transferred into Teflon-lined stainless steel autoclaves with a capacity of 40 cm^3 , which were heated statically at 423 K under autogeneous pressure for 5 days.

The resulting solids were collected by centrifugation, washed with water and ethanol and dried at room temperature overnight. The organic template and the water trapped within the micropores of the as-synthesized solids were removed by calcination at 823 K prior to catalyst testing. Complete removal of the organic molecule was assessed by thermogravimetric analysis.

2.2. Characterization

Powder X-ray diffraction (XRD) patterns of as-synthesized and calcined samples were recorded on a Philips X'PERT diffractometer using $\text{CuK}\alpha$ radiation with a nickel filter. The textural data (pore volume and BET surface area) were determined by nitrogen adsorption/desorption measurement using a Micrometrics ASAP 2010 volumetric apparatus. Previous to measure the nitrogen adsorption/desorption isotherms samples were degassed at 623 K under vacuum for at least 20 h. The crystal size and morphology were examined by scanning electron microscopy (SEM) using a JEOL JSM 6400 or a Philips XL30 microscope, operating at 20 kV. Elemental mapping by EDX

has carried out using a ultrahigh resolution FEI-NOVA NanoSEM 230 FESEM instrument.

The organic content of the samples was determined by elemental analysis with a Perkin-Elmer 2400 CHN analyser and by thermogravimetric analysis (TGA) using a Perkin-Elmer TGA7 instrument. TG analyses were carried out at a heating rate of 20 K/min under air flow. Chemical analysis of Al, P and Si in calcined samples was performed by inductively coupled plasma optical emission spectrometry (ICP-OES, Perkin-Elmer 3300DV instrument) after sample dissolution by alkaline fusion.

^{29}Si CP/MAS NMR spectra were recorded at room temperature using a Bruker AV-400-WB spectrometer operating at 79.5 MHz, with a 4 mm probe spinning at 10 kHz. A $\pi/2$ pulse of 3 μs , contact time of 6 ms and recycle delay of 5 s were used. The chemical shifts were referenced to tetramethylsilane (TMS), taken as 0 ppm.

Ammonia temperature programmed desorption (NH_3 -TPD) was performed using a Quantachrome ChemBET-3000 TPR/TPD equipment. Typically, 100 mg of sample pellets (20–40 mesh) were pre-treated at 823 K for 1 h in helium flow (25 mL/min) and subsequently cooled to the adsorption temperature (400 K). A gas mixture of 5.0 vol% NH_3 in He was then allowed to flow over the sample for 4 h at a rate of 15 mL/min. Afterwards, a 25 mL/min helium flow was passed over the sample, while maintaining the temperature at 400 K for 30 min to remove weakly adsorbed NH_3 , and, finally, the temperature was increased to 823 K at a rate of 10 K/min.

2.3. Catalyst testing

Methanol conversion to olefins was tested at 623, 673 and 723 K using a laboratory plant with a continuous down flow packed bed reactor, fully automated and controlled from a personal computer (PiD Eng&Tech Microactivity Reference), operating at atmospheric pressure. Catalyst weight (1.0 g; 20–30 mesh pellets size) and methanol flow rate (0.025 ml/min) were adjusted in order to obtain a weight hourly space velocity (WHSV) of 1.2 h^{-1} . Previous to the reaction, samples were pre-treated under nitrogen flow at 723 K for 1 h. During the reaction, nitrogen was used as an inert diluent gas and co-fed with methanol into the reactor with a constant methanol/nitrogen ratio of 1/1 mol. Methanol was fed as liquid using a Gilson 307 HPLC pump, vaporized and mixed with the nitrogen stream in a pre-heater at 473 K. The reaction products were analyzed on-line by gas chromatography using a Varian CP3800 gas chromatograph equipped with flame ionization (FID) and thermal conductivity (TCD) detectors, with a Petrocol DH50.2 capillary column and a Porapack Q 80–100 mesh packed column for separation of hydrocarbons and oxygenates, respectively.

3. Results and discussion

3.1. Crystal structure and morphological analysis

The synthesis conditions were varied in order to obtain SAPO-34 crystals using a dilute solution. The molar composition of the reaction mixtures and the synthesis conditions for the different materials obtained are given in Table 1. A sample prepared with aluminium hydroxide [21] is also included as a reference material. Relatively large amounts of template (tetraethylammonium hydroxide) were used in order to neutralize the hydrochloric acid released into the medium due to hydrolysis of aluminium chloride, for SAPO-34 crystallization is favoured around neutral pH. Initially, the amount of template was increased from the TEAOH/Al₂O₃ ratio of 1 used in the conventional synthesis method to a ratio of 3. Although the amount of TEAOH used was high, the pH of the synthesis gel (1.4) was too acidic to allow the SAPO-34 material to

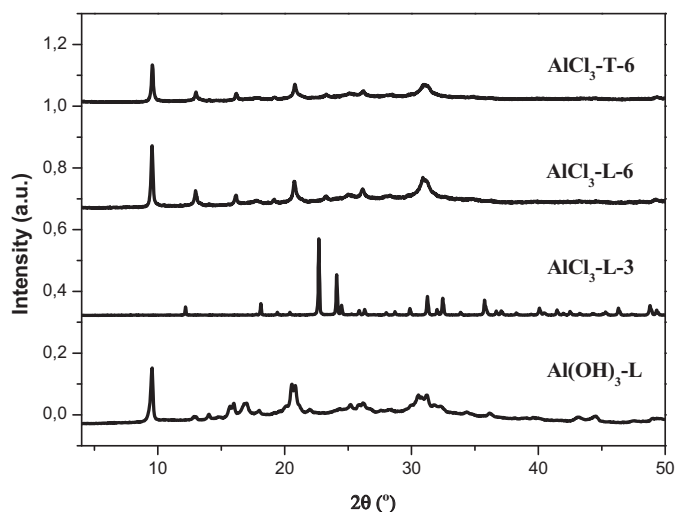


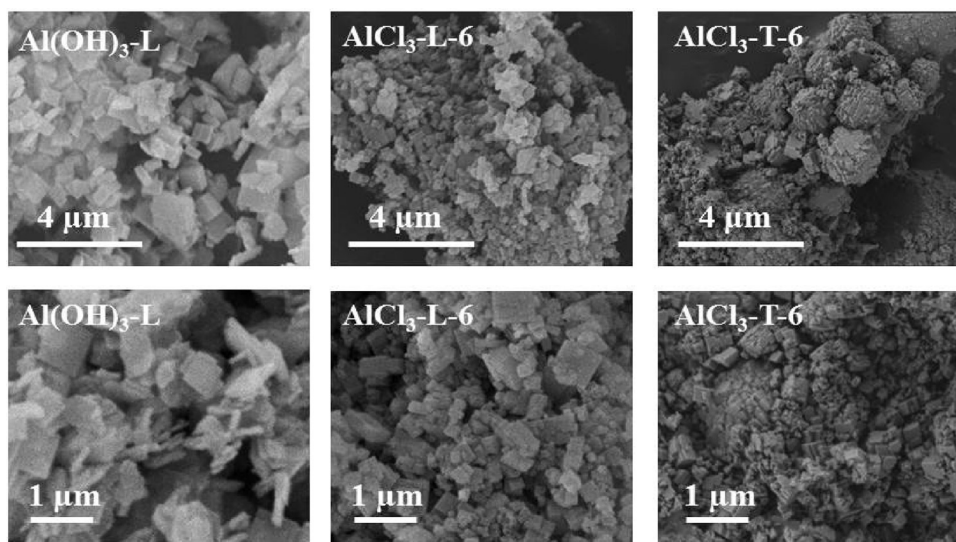
Fig. 1. XRD patterns of as-synthesized samples.

crystallize and only a dense phase was obtained, as indicated by the XRD pattern of sample AlCl₃-L-3 (Fig. 1). Therefore, the ratio was increased to TEAOH/Al₂O₃ = 6 in order to reach a pH value suitable for the crystallization of the desired material. With this new composition two gels were prepared using two different silicon sources, Ludox and TEOS, to study its effect on the physico-chemical properties of the resulting material. The X-ray powder diffraction patterns (Fig. 1) confirmed the structure type SAPO-34 (CHA framework code) for both as-synthesized samples, AlCl₃-L-6 and AlCl₃-T-6, according to patterns reported for this structure [35]. Nevertheless, slight differences respect to the pattern of the reference sample Al(OH)₃-L can be observed (Fig. 1), which can be attributed to different crystallite shape and size for both types of samples. Practically no loss of crystallinity was observed when the as-synthesized samples were heated at 823 K in order to remove the organic molecules (Supplementary Information, Fig. I), confirming their thermal stability under calcination conditions. The XRD patterns of the two samples prepared with aluminium chloride using different silicon sources exhibit comparable peak width. This fact suggests that both samples present similar crystal size.

Some selected scanning electron microscopy (SEM) photographs of the SAPO-34 materials synthesized are presented in Fig. 2. It is observed that samples prepared with aluminium chloride have very similar morphology, although the sample prepared with TEOS (AlCl₃-T-6) possesses slightly smaller crystal size. In the micrographs, the typical cubic-like rhombohedra morphology can be clearly observed, with crystals approximately 200–300 nm in size. However, the sample prepared with aluminium hydroxide (Al(OH)₃-L) presents a quite different crystal shape and size. As it can be observed in the micrographs, sample Al(OH)₃-L presents plate-like crystals with size around 500 nm × 300 nm and several tenths of nm thickness. Therefore, it was found that using highly diluted precursor solution (samples AlCl₃-L-6 and AlCl₃-T-6, prepared with aluminium chloride) the crystal size of this material can be decreased.

3.2. Thermogravimetric and elemental analysis

Thermogravimetric analyses (TGA) were performed aiming to verify the incorporation of the SDA molecules in the structure of the as-made samples and their subsequent complete elimination after calcination prior to the use of SAPO-34 materials in the catalytic reactions. The TGA profiles of the samples studied are plotted in Fig. 3. These results show three different weight loss

**Fig. 2.** SEM images of calcined samples.**Table 2**
Elemental (CNH) and thermogravimetric analyses of the as-synthesized samples.

Sample	Weight loss (%) ^a			Organic content ^b		
	I ($T < 473$ K)	II ($473 < T < 823$ K)	III (> 823 K)	wt (%)	C/N Exper.	Template molec. per cage
Al(OH) ₃ -L	3.1	14.2	1.8	13.9	7.34	1.00
AlCl ₃ -L-6	6.4	11.5	2.8	14.3	7.26	1.07
AlCl ₃ -T-6	6.7	14.4	1.5	14.6	7.31	1.06

^a From TGA analyses.^b From chemical analyses.

steps. The first weight loss (I), at temperatures below 473 K, can be attributed to removal of adsorbed water. The second weight loss (II), between 473 K and 823 K, is due to the decomposition of the template. Finally, the third weight loss (III), at temperatures higher than 823 K, is associated with the combustion of organic residues occluded in the channels and cages of the SAPO-34. Quantitative data of the different weight losses are presented in **Table 2**.

The derivative plot presented in **Fig. 3** shows that the kinetics of template removal in sample Al(OH)₃-L is markedly different from that of samples obtained with AlCl₃. In samples prepared with aluminium chloride, the profile exhibits a single peak centred at 723 K that can be associated to decomposition of tetraethylammonium species. In contrast, the profile of sample Al(OH)₃-L reveals,

at least, three different steps in the temperature range from ca. 623 K to 773 K. These results suggest that there is a different interaction between the organic cations and the SAPO framework in both types of samples, and that part of the organic occluded in the pores of sample Al(OH)₃-L is more weakly bonded to the inorganic network. On the other hand, it is observed that the weight loss at temperatures below 473 K is higher for samples prepared with aluminium chloride. Therefore, these samples show a more hydrophilic behaviour than sample Al(OH)₃-L.

The total weight losses of steps II and III are in good agreement with the organic content determined by CHN elemental analysis (**Table 2**), confirming the previous assignment of weight losses II and III to removal of template. Moreover, the C/N ratios determined by elemental analysis are very close to 8, the value corresponding to TEAOH, which indicates that the organic SDA molecules occluded or adsorbed in the different samples were not decomposed during the hydrothermal treatment. Based on the topological structure of SAPO-34 molecular sieve, the average number of template molecules per cage in the different samples was calculated (**Table 2**). In all the cases the organic content corresponds to one molecule of SDA (TEAOH) incorporated per unit cell.

The chemical composition of samples obtained by ICP-OES is presented in **Table 3**. In samples prepared with aluminium chloride, the Si/Al+P ratio is very close to that of the synthesis gels, and this value is slightly higher for sample Al(OH)₃-L. Although the amount of silicon incorporated in the network is similar for AlCl₃-L-6 and AlCl₃-T-6, the different proportion of phosphorous and aluminium in the solids suggests that the silicon distribution in the framework is rather different in both samples. This will be discussed later on the basis of ²⁹Si-NMR analysis. EDX elemental mapping of the three samples was also collected (Figs. III–V and Table I of Supplementary Information). Oxygen, aluminium, silicon and phosphorus were detected. The distribution of the elements was very

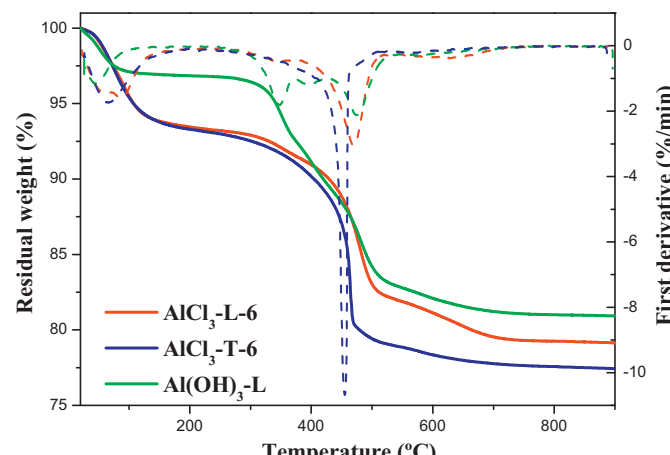
**Fig. 3.** Thermogravimetric analyses of SAPO-34 samples.

Table 3
Elemental composition.

Sample	Molar composition	Si/(Al+P) _{gel}	Si/(Al+P) _{solid}	Si incorporation ^a	NH ₃ TPD (mmol/g)
Al(OH) ₃ -L	Si _{0.17} Al _{0.43} P _{0.40} O ₂	0.15	0.20	1.31	0.43
AlCl ₃ -L-6	Si _{0.13} Al _{0.48} P _{0.39} O ₂	0.15	0.15	1.00	0.64
AlCl ₃ -T-6	Si _{0.13} Al _{0.40} P _{0.47} O ₂	0.15	0.15	1.00	0.67

^a The level of silicon incorporation is defined as the molar ratio: [Si/(Si+Al+P)]_{solid}/[Si/(Si+Al+P)]_{gel}.

homogenous on the entire particles of the samples with lower Si content. The contents of Si, Al and P determined by both techniques, EDX and ICP-OES, are very similar in the case of samples AlCl₃-L-6 and AlCl₃-T-6. However, for sample Al(OH)₃-L, the amount of silicon obtained by EDX, is slightly lower than that determined by ICP-OES. This result might indicate that the later sample contains a small amount of amorphous silica, which would contribute to the total silicon content determined by ICP-OES but would not be detected in a local analysis of crystals by EDX.

3.3. Textural properties

Calcined materials were analyzed by nitrogen adsorption-desorption at 77 K in order to determine their textural properties. All the samples possess an important microporous contribution, typical of these kind of materials, and a smaller, but significant, external one (Fig. II in Supplementary Information). Pore volume and surface area values calculated from the isotherms are collected in Table 4. It can be observed that all the samples have surface area in the range 620–650 m²/g. However, it should be noticed that the non microporous component, both in surface area and volume, is significantly higher for sample AlCl₃-T-6. These differences can be attributed to a smaller crystal size and higher intercrystalline porosity of the sample synthesized with TEOS as silicon source.

3.4. ²⁹Si MAS NMR

The incorporation of Si to the SAPO-34 framework has been studied by ²⁹Si MAS NMR (Fig. 4). It has been reported that, when the amount of silicon incorporated to the SAPO framework is low, Si atoms are found in a unique Si(4Al) environment resulting from the substitution of phosphorous by silicon in the aluminophosphate framework [36]. However, if the silicon content is higher, multiple silicon environments can occur as a result of the combination of the single P by Si substitution mechanism with the simultaneous substitution of a pair of neighbouring Al and P atoms by two Si atoms. This can be observed in Fig. 4, where various distinct resonances can be distinguished in the range –87 to –110 ppm, attributed to different Si(nAl) environments ($n=0\text{--}4$). Sample AlCl₃-L-6 presents a broad band centred at –87 ppm attributed to Si(4Al) environments, corresponding to Si atoms in phosphorous positions, although this band has a certain asymmetry, showing a small contribution to lower field. This suggests the presence of a small fraction of Si in Si(nAl) environments with n lower than 4. Therefore the silicon substitution is occurring mainly via mechanism 2 (SM2: a phosphorous atom substituted by a silicon atom). This mechanism leads to Si surrounded by 4 Al atoms in the second coordination shell, and

creates a negative charge per every Si atom in the framework, which is usually balanced by the positive charge of the organic molecules occluded within the microporous structure. However, in the case of sample AlCl₃-T-6, in addition to this band, centred at –87 ppm, other signals can be observed at –94 ppm and –99 ppm, and also, with lower intensity, at –105 ppm and –110 ppm, which have been previously attributed to Si(3Al), Si(2Al), Si(1Al) and Si(0Al), respectively. The presence of these bands can be explained if silicon is incorporated into the framework via substitution mechanism 3 (SM3), in which the incorporation of Si occurs via a simultaneous substitution of a pair of adjacent Al and P atoms by two Si atoms. The higher intensity of the resonances appearing at lower field in sample AlCl₃-T-6 compared to sample AlCl₃-L-6 indicates a higher contribution of substitution mechanism SM3 in the former sample which should result in a lower Al/P ratio, in agreement with the chemical analysis results (Table 3). Sample Al(OH)₃-L presents a spectrum clearly different from the other samples, with a more intense signal at –110 ppm, indicating aluminosilicate domains (commonly referred to as Si islands) in the SAPO network [37–39]. Depending on the relative contribution of both SM3 and SM2 substitution mechanisms, the size and concentration of Si islands will be different [40–42]. Some authors have proposed that the strength of the acid sites generated at the border of the Si islands is higher than that of the acid sites created by the isolated Si atoms, and that the strength increases as the value of n in the Si(OAl)_n(OSi)_{4-n} environments decreases [40]. Thus, a higher number of acid sites are generated through the SM2 mechanism, while substitution via SM2+SM3 yields less but stronger acid sites. Therefore, according to spectra shown in Fig. 4, it can be expected that sample AlCl₃-T-6 has acid sites with higher strength on average than sample AlCl₃-L-6, due its lower proportion of isolated Si atoms. Furthermore, sample Al(OH)₃-L would possess the strongest acid sites as its ²⁹Si NMR spectrum indicates that it contains the largest proportion of acid sites at the border of Si islands.

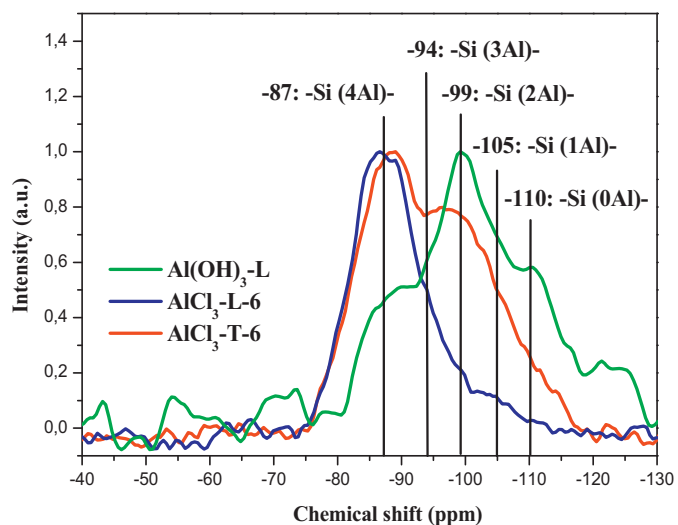


Table 4
Textural properties of calcined materials.

Sample	Surface area (m ² /g)			Pore volume (cm ³ /g)		
	S _{micro}	S _{ext}	S _{total}	V _{micro}	V _{ext}	V _{total}
S-Al(OH) ₃ -L	608	44	652	0.26	0.29	0.55
S-AlCl ₃ -L-6	588	31	619	0.25	0.17	0.42
S-AlCl ₃ -T-6	558	76	633	0.23	0.36	0.59

Fig. 4. ²⁹Si CP/MAS NMR spectra of calcined samples.

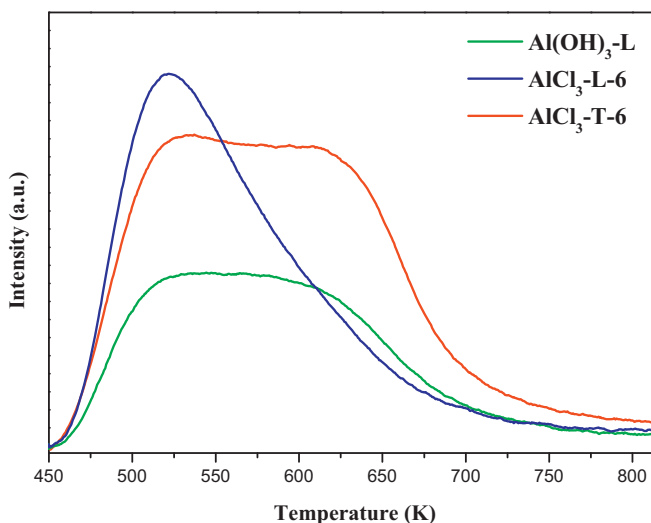


Fig. 5. NH₃-TPD plots of calcined SAPO-34 catalysts.

3.5. Acidity

The acidity of the catalysts has been evaluated by TPD of ammonia (Fig. 5 and Table 3). The area under the TPD profile indicates the total amount of ammonia desorbed, which is equivalent to the number of acid sites, whereas the desorption temperature indicates the acid strength of the sites, the desorption temperature increasing with the acid site strength. The three SAPO-34 samples show different TPD profiles. Sample AlCl₃-L-6 presents a major desorption peak at low temperature (with maximum at around 525 K), which is an indication of site uniformity and of a relatively weak acid strength. The TPD profile shows some tailing towards higher temperatures, indicating the presence of a small proportion of acid sites with higher strength. However, samples AlCl₃-T-6 and Al(OH)₃ exhibit broader desorption profiles, clearly showing an important contribution of a desorption band with maximum at around 610 K, corresponding to strong acid sites, overlapping with the low temperature ammonia desorption peak attributed to weak acid sites. These results are in agreement with the ²⁹Si NMR results described previously. The spectrum of sample AlCl₃-L-6 presents a broad band centred at -87 ppm attributed to Si(4Al) environments, which give rise to bridging Si-OH-Al hydroxyl groups of weak acid strength, in accord with the presence of mainly a low temperature desorption peak at in the ammonia TPD. In contrast, the ²⁹Si NMR spectra of samples AlCl₃-T-6 and Al(OH)₃-L show an important contribution of bands assigned to Si(3Al), Si(2Al) and Si(1Al) environments. The bridging Si-OH-Al hydroxyl groups associated to silicon atoms located in those environments are expected to exhibit stronger acidity, and would be responsible for the presence of the high temperature band in the TPD of ammonia. On the other hand, silicon atoms in Si(0Al) environments, that is, surrounded by 4 silicon atoms, do not contribute to the formation of acidic hydroxyl groups. Accordingly, the higher proportion of these Si centres found in sample Al(OH)₃-L might explain its lower overall content of acid sites determined by ammonia TPD (Table 3).

3.6. Catalytic activity

The catalytic activity of these materials in the MTO reaction was studied at 623, 673 and 723 K and a WHSV of 1.2 h⁻¹ as it has been described previously in Section 2 (Figs. 6 and 7). It can be observed that samples prepared with aluminium chloride had a very similar stability in the MTO reaction at the different temperatures studied and this stability was always higher than that shown by sample

Al(OH)₃-L. This improved performance of the catalysts prepared with aluminium chloride can be attributed to their smaller crystal size compared to sample Al(OH)₃-L.

The catalysts performance was strongly dependent on the reaction temperature used. At 623 K, all catalysts showed a very short lifetime reaching high conversion levels during two hours or less and showing subsequently a fast decay of conversion. At higher temperatures the results were quite different. Samples AlCl₃-L-6 and AlCl₃-T-6 rendered complete conversion of oxygenates (both methanol and dimethylether) and high selectivity towards short chain olefins (C₂=–C₄=) during 6 h at 673 and 723 K. However, the catalyst lifetime decreased when the temperature was increased from 673 to 723 K. At 673 K, the conversion was maintained above 80% during 10 h while at 723 K, conversion levels were lower than 70% after 7 h of reaction. These results can be explained assuming that deactivation of acid sites due to formation of heavy hydrocarbon species takes place first for the strongest sites. After deactivation of the strong acid sites in the initial period of reaction, the remaining weaker sites would not be active enough to catalyze the transformation of DME to olefins at 623 K, which would explain the decrease of conversion observed at this temperature after a short time of reaction. At higher reaction temperature (673 K), the less acidic sites would be able to transform DME into light olefins, thus increasing the catalyst lifetime. A further increase of temperature to 723 K decreases the lifetime due to a faster deactivation of the catalyst, as the formation of pore-blocking products in the course of the reaction would be enhanced, making the active sites of the catalyst less accessible for reactant molecules.

The main problem of this kind of catalysts in the MTO process is the rapid deactivation attributed to the deposition of high molecular weight hydrocarbons on the pore entrances [7,43,44]. However, it is possible to optimize the synthesis of these materials to improve the catalyst lifetime [45–48]. At all the temperatures tested, samples prepared with aluminium chloride retained high conversion during more time than the conventional sample. There are several factors that could explain the poorer behaviour of the conventional sample compared with these new materials. First, this sample has higher Si content in the solid and higher proportion of Si(nAl) environments with *n* equal to 2 or 1. These Si species are associated to acid centres with higher acid strength [49] and, therefore, are responsible for the transformation of short chain olefins to higher molecular weight compounds, which causes the catalyst deactivation. The second factor affecting the stability of the catalyst is the larger crystal size of this sample, which has been also correlated with a lower resistance of the catalysts to deactivation [9,19,21].

All the catalysts gave selectivity to light olefins up to ca. 90% at conversion levels close to 100% (Fig. 7). The decrease of conversion was accompanied by a decrease of the selectivity to light olefins that was more pronounced at 723 K. These results can be attributed to the deactivation of acid sites, which leads to the formation of important amounts of methane and aromatics at long time of reaction, especially at 723 K.

For all the catalysts, the ethylene/propylene ratio increased with the reaction temperature (Fig. 8). During the period of high conversion of oxygenates, this ratio was around 0.7 at 623 K, 1.0 at 673 K and 1.6 at 723 K. The raise in ethylene/propylene ratio with temperature has been previously attributed to the secondary reactions of oligomerization and cracking, which are favoured when the reaction temperature increases [50,51]. Some differences among the catalysts could be observed in the distribution of the reaction products. The ethylene/propylene ratio was slightly higher for sample AlCl₃-T-6 than for sample AlCl₃-L-6. This result can be attributed to the fact that the sample prepared with TEOS possesses stronger acid sites (as ²⁹Si NMR and TPD of ammonia results indicate), which favours the cracking of heavy compounds to light olefins, leading to higher amounts of ethylene than propylene.

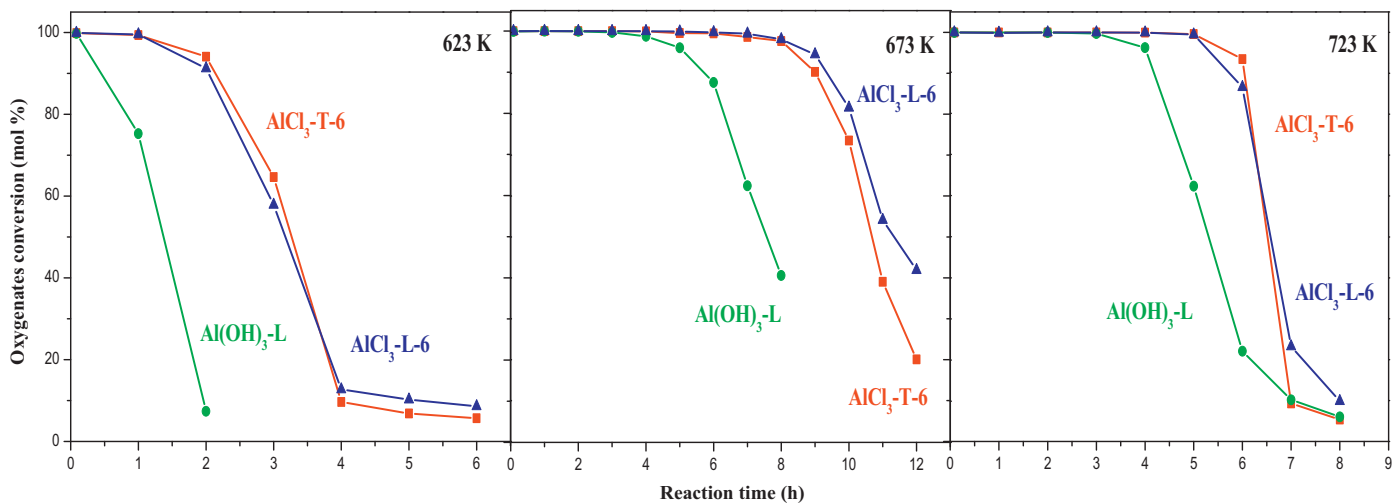


Fig. 6. Conversion of oxygenates (MeOH and DME) vs. reaction time. Test conditions: $T = 623, 673$ and 723 K, WHSV = 1.2 h^{-1} , 1 g of catalyst.

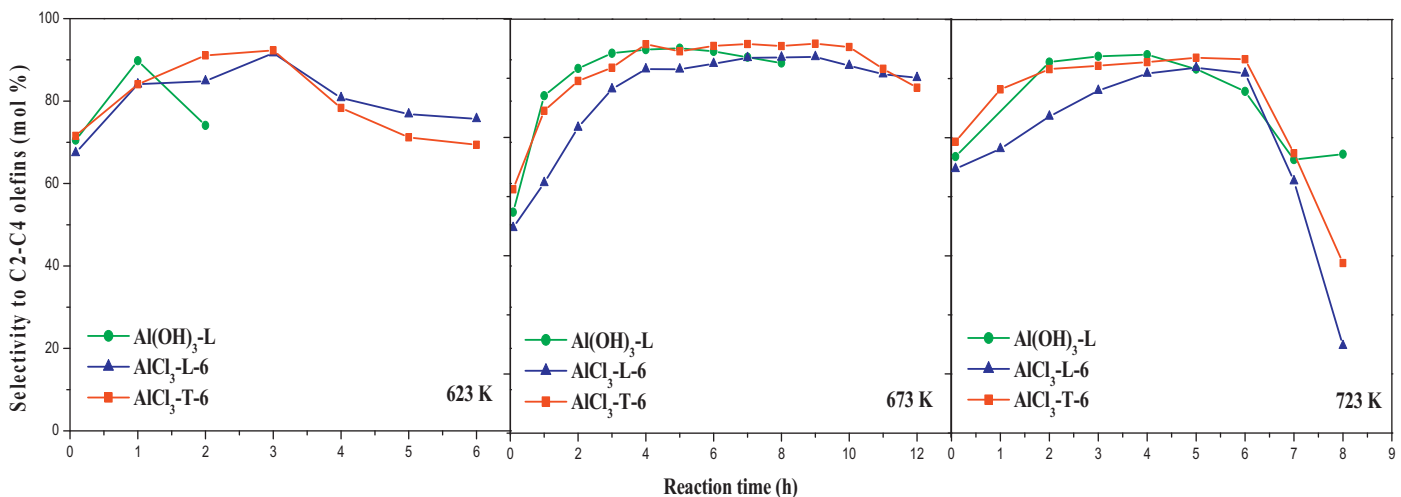


Fig. 7. Selectivity to short chain olefins (C₂-C₄) in the MTO reaction as a function of time-on-stream. Test conditions: $T = 623, 673$ and 723 K, WHSV = 1.2 h^{-1} , 1 g of catalyst.

From the results presented here, it can be concluded that the crystal size of SAPO-34 catalysts would be the main parameter to control the catalytic behaviour in order to obtain more stable materials with longer lifetime. Moreover, it is necessary to obtain

materials with the appropriate proportion of Si(*n*Al) environments, associated to acid sites of moderate acid strength, to maximize the transformation of methanol to light olefins while limiting the transformation of short olefins to higher molecular weight compounds.

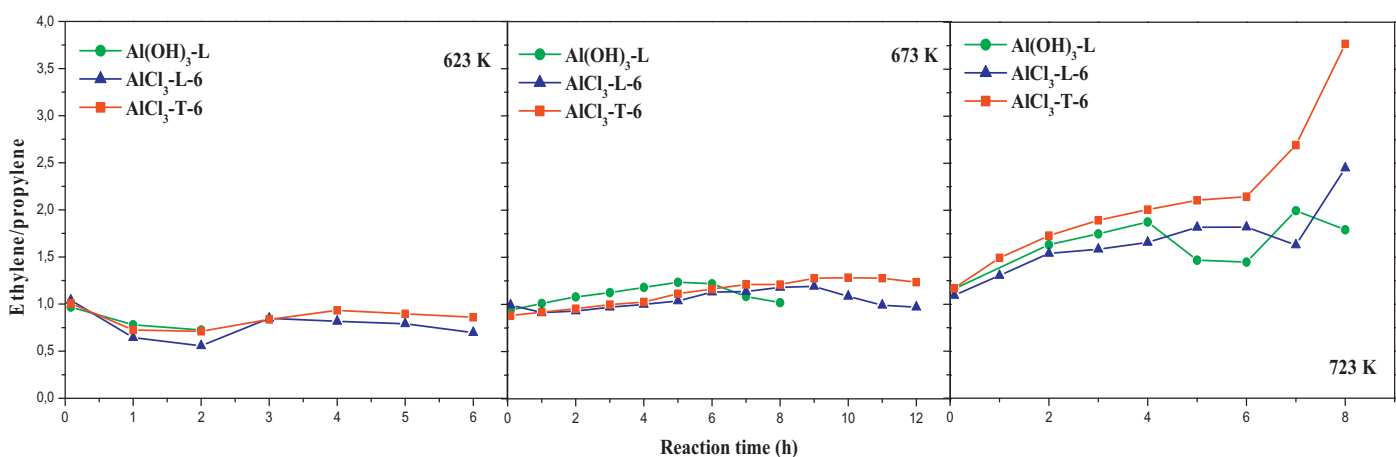


Fig. 8. Ethylene/propylene ratio obtained in the MTO reaction at different temperatures as a function of time-on-stream. Test conditions: $T = 623, 673$ and 723 K, WHSV = 1.2 h^{-1} , 1 g of catalyst.

The results demonstrate that samples synthesized with aluminium chloride, which present smaller crystal size, rendered the best catalytic performance.

4. Conclusions

SAPO-34 catalysts have been synthesized using aluminium chloride. Using highly diluted precursor solutions the crystal size of this material can be decreased. This method provided rhombohedral crystals with dimensions of 200–300 nm, while an optimized sample prepared by the conventional procedure was formed by plate-like crystals with size around 300 nm × 500 nm and several tenths of nm thickness. It was shown that this decrease in the crystal size was the main factor allowing to obtain materials with improved catalytic performance in the MTO process, which retain high conversion of oxygenates for longer reaction time.

Acknowledgements

We are thankful for the financial support of the Spanish Ministry of Economy and Competitiveness, project MAT2012-31127. TAM acknowledges CSIC for a PhD grant.

Appendix A. Supplementary data

Supplementary material related to this article can be found, in the online version, at <http://dx.doi.org/10.1016/j.apcata.2013.12.016>.

References

- [1] A. Gotti, R. Prins, J. Catal. 178 (1998) 511–519.
- [2] I. Wender, Fuel Process. Technol. 48 (1996) 189–297.
- [3] C.V. Ovesen, B.S. Clausen, J. Schiotz, P. Stoltze, H. Topsoe, J.K. Norskov, J. Catal. 168 (1997) 133–142.
- [4] G.A. Olah, A. Goeppert, G.K.S. Prakash, J. Org. Chem. 74 (2009) 487–498.
- [5] C. Song, Catal. Today 115 (2006) 2–32.
- [6] C.N. Hamelinck, A.P.C. Faaji, J. Power Sources 111 (2002) 1–22.
- [7] J. Liang, H. Li, S. Zhao, W. Guo, R. Wang, M. Ying, Appl. Catal. 64 (1990) 31–40.
- [8] M. Stöcker, Microporous Mesoporous Mater. 29 (1999) 3–48.
- [9] D. Chen, K. Moljord, T. Fuglerud, A. Holmen, Microporous Mesoporous Mater. 29 (1999) 191–203.
- [10] S. Wilson, P. Barger, Microporous Mesoporous Mater. 29 (1999) 117–126.
- [11] T.V.W. Janssens, S. Svelle, U. Olsbye, J. Catal. 308 (2013) 122–130.
- [12] D. Mores, J. Kornatowski, U. Olsbye, B.M. Weckhuysen, Chem. Eur. J. 17 (2011) 2874–2884.
- [13] D. Mores, E. Stavitski, M.H.F. Kox, J. Kornatowski, U. Olsbye, B.M. Weckhuysen, Chem. Eur. J. 14 (2008) 11320–11327.
- [14] D.S. Wragg, M.G. O'Brien, F.L. Bleken, M. DiMichiel, U. Olsbye, H. Fjellvåg, Angew. Chem. Int. Ed. 51 (2012) 7956–7959.
- [15] A.T. Aguayo, A.E.S. del Campo, A.G. Gayubo, A. Tarrío, J. Bilbao, J. Chem. Technol. Biotechnol. 74 (1999) 315–321.
- [16] D. Chen, H.P. Rebo, K. Moljord, A. Holmen, Ind. Eng. Chem. Res. 38 (1999) 4241–4249.
- [17] A.J. Marchi, G.F. Froment, Appl. Catal. 71 (1991) 139–152.
- [18] M.J. van Niekerk, J.C.Q. Fletcher, C.T. O'Connor, Appl. Catal. 138 (1996) 135–145.
- [19] N. Nishiyama, M. Kawaguchi, Y. Hirota, D. Van Vu, Y. Egashira, K. Ueyama, Appl. Catal. A: Gen. 362 (2009) 193–199.
- [20] K.Y. Lee, H.-J. Chae, S.-Y. Jeong, G. Seo, Appl. Catal. A: Gen. 369 (2009) 60–66.
- [21] T. Álvaro-Muñoz, C. Márquez-Álvarez, E. Sastre, Catal. Today 179 (2012) 27–34.
- [22] Y. Hirota, K. Murata, M. Miyamoto, Y. Egashira, N. Nishiyama, Catal. Lett. 140 (2010) 22–26.
- [23] J. Yao, H. Wang, S.P. Ringer, K.-Y. Chan, L. Zhang, N. Xu, Microporous Mesoporous Mater. 85 (2005) 267–272.
- [24] H.Q. Yang, Z.C. Liu, H.X. Gao, Z.K. Xie, J. Mater. Chem. 20 (2010) 3227–3231.
- [25] S.T. Yang, J.Y. Kim, H.J. Chae, M. Kim, S.Y. Jeong, W.S. Ahn, Mater. Res. Bull. 47 (2012) 3888–3892.
- [26] F. Schmidt, S. Paasch, E. Brunner, S. Kaskel, Microporous Mesoporous Mater. 164 (2012) 214–221.
- [27] H. van Heyden, S. Mintova, T. Bein, Chem. Mater. 20 (2008) 2956–2963.
- [28] C.S. Cundy, J.O. Forrest, Microporous Mesoporous Mater. 72 (2004) 67–80.
- [29] J.-W. Jun, J.-S. Lee, H.-Y. Seok, J.-S. Chang, J.-S. Hwang, S.-H. Jhung, Bull. Korean Chem. Soc. 32 (2011) 1957–1964.
- [30] C. Gabriel, S. Gabriel, E.H. Grant, E.H. Grant, B.S.J. Halstead, D. Michael, P. Mingos, Chem. Soc. Rev. 27 (1998) 213–223.
- [31] S.-E. Park, D.S. Kim, J.-S. Chang, W.Y. Kim, Catal. Today 44 (1998) 301–308.
- [32] X. Xu, W. Yang, J. Liu, L. Lin, Adv. Mater. 12 (2000) 195–198.
- [33] D.P. Serrano, M.A. Uguina, R. Sanz, E. Castillo, A. Rodríguez, P. Sánchez, Microporous Mesoporous Mater. 69 (2004) 197–208.
- [34] L. Tosheva, V.P. Valtchev, Chem. Mater. 17 (2005) 2494–2513.
- [35] B.M. Lok, C.A. Messina, R.L. Patton, R.T. Gajek, T.R. Cannan, E.M. Flanigen, US Patent 4,440,871 (1984).
- [36] C.S. Blackwell, R.L. Patton, J. Phys. Chem. 88 (1984) 6135–6139.
- [37] L. Xu, A. Du, Y. Wei, Y. Wang, Z. Yu, Y. He, X. Zhang, Z. Liu, Microporous Mesoporous Mater. 115 (2008) 332–337.
- [38] A. Izadbakhsh, F. Farhadi, F. Khorasheh, S. Sahebdelfar, M. Asadi, Z.F. Yan, Microporous Mesoporous Mater. 126 (2009) 1–7.
- [39] J. Tan, Z. Liu, X. Bao, X. Liu, X. Han, C. He, R. Zhai, Microporous Mesoporous Mater. 53 (2002) 97–108.
- [40] S. del Val, T. Blasco, E. Sastre, J. Pérez-Pariente, J. Chem. Soc., Chem. Commun. (1995) 731–732.
- [41] J.A. Martens, C. Janssens, P.J. Grobet, H.K. Beyer, P.A. Jacobs, Stud. Surf. Sci. Catal. 49 (1989) 215–225.
- [42] A.M. Prakash, S. Unnikrishnan, K.V. Rao, Appl. Catal. A: Gen. 110 (1994) 1–10.
- [43] A. Gronvold, K. Moljord, T. Dypvik, A. Holmen, Stud. Surf. Sci. Catal. 81 (1994) 399–404.
- [44] D. Chen, H.P. Rebo, A. Gronvold, K. Moljord, A. Holmen, Microporous Mesoporous Mater. 35–36 (2000) 121–135.
- [45] P.F. Wang, A.L. Lv, J. Hu, J.A. Xu, G.Z. Lu, Microporous Mesoporous Mater. 152 (2012) 178–184.
- [46] T. Álvaro-Muñoz, C. Márquez-Álvarez, E. Sastre, Catal. Today 213 (2013) 219–225.
- [47] H.-G. Jang, H.-K. Min, J.K. Lee, S.B. Hong, G. Seo, Appl. Catal. A: Gen. 437–438 (2012) 120–130.
- [48] T. Álvaro-Muñoz, C. Márquez-Álvarez, E. Sastre, Catal. Today 215 (2013) 208–215.
- [49] G. Sastre, D.W. Lewis, J. Chem. Soc., Faraday Trans. 94 (1998) 3049–3058.
- [50] M. Popova, C. Minchev, V. Kanazirev, Appl. Catal. A: Gen. 169 (1998) 227–235.
- [51] X. Wu, M.G. Abraha, R.G. Anthony, Appl. Catal. A: Gen. 260 (2004) 63–69.